The deaminase ADAL-pivoted catabolism checkpoint suppresses aberrant DNA N6-methyladenine incorporation

Shaokun Chen
University of Chinese Academy of Sciences
Weiyi Lai
Chinese Academy of Sciences
Zhiyi Zhao
University of Chinese Academy of Sciences
Ning Zhang
Chinese Academy of Sciences
Yan Liu
Chinese Academy of Sciences
Xiangjun Li
University of Chinese Academy of Sciences
Guibin Jiang
Research Center for Eco-Environmental Sciences, Chinese Academy of Sciences
Hailin Wang (HLWang@rcees.ac.cn)
Chinese Academy of Sciences

Article

Keywords: epigenetics, RNA N6-methyladenine (m6A)

Posted Date: April 13th, 2021

DOI: https://doi.org/10.21203/rs.3.rs-374831/v1

Abstract

Abundant RNA N^6-methyladenine (m6A) is degraded in RNA decay and potentially induces aberrant DNA N^6-methyladenine (6mA) misincorporation. Biophysically, like truly methylated product DNA 6mA, misincorporated 6mA also destabilizes the DNA double helix and thus ditto affects DNA replication and transcription. By heavy stable isotope tracing, we demonstrate that intracellular degradation of RNA m6A cannot induce any misincorporated DNA 6mA, unveiling the existence of a catabolism checkpoint that blocks DNA 6mA misincorporation. We further show that the deaminase ADAL preferentially catabolizes N^6-methyl-2'-deoxyadenosine monophosphate (6mdAMP) *in vitro* and *in vivo*, and adenylate kinase 1 restricts the phosphorylation rate of 6mdAMP, together contributing to the identified checkpoint. Noteworthy, low ADAL expression reduces dramatically the patient survival in four cancers. Collectively, our data strongly support a pivotal role of ADAL in the suppression of 6mA misincorporation and implicate that both ADAL and misincorporated 6mA may mark cancer abnormalities.

Introduction

As a prevalent DNA epigenetic modification in prokaryotes[1–4] and some single-cellular eukaryotes[5,6], DNA N^6-methyl-2'-deoxyadenosine (6mA) is also found or proposed to exist in multicellular eukaryotes such as fungi[7], C. elegans[8], Drosophila[9], plants[10,11], vertebrates[12], and mammals[12–16]. Despite its low abundance, eukaryotic DNA 6mA has a number of potential functions regulating gene transcription[5,8], transposon activity[9,10,16], nucleosome occupancy[6,17,18], and transgenerational progression[19–22]. Biochemically, the presence of the N^6-methyl group on adenine of the DNA template induces RNA pol II pausing[23] and partially inhibits DNA replication[24].

Meanwhile, epigenetic mRNA N^6-methyladenosine (m6A), which shares the same N^6-methyladenine base with DNA 6mA, is one of the most abundant internal posttranscriptional modifications in mammals. mRNA m6A is highly enriched in 3□ untranslated regions, stop codon flanking regions, and long internal exons of mRNA[25–27] and regulates transcription and processing in the nucleus and translation and decay in the cytoplasm[28–31]. Notably, as a prevalent activity RNA degrades, and the half-life of mRNA is generally as short as minutes to hours[32–35]. Introns and spacer sequences in mRNA during processing; defective mRNA fragments during transcription, processing, and functioning; and scrapped mature mRNAs are degraded as signaling by a surveillance system[36–38]. Along with mRNA degradation, unmodified adenosine phosphates are released into nucleotide pools and then partly converted into reusable 2'-deoxyadenosine triphosphate (dATP) through purine salvaging[39]. Similarly, substantial m6A-related species (e.g., N^6-methyladenosine monophosphate (m6AMP)[40]) are released to the nucleotide pools. It is expected that following purine salvage, the released m6A-related species might be ultimately converted into N^6-methyl-2'-deoxyadenosine triphosphate (6mdATP), which can be misincorporated into genomic DNA by DNA polymerases[13,41] and result in the generation of DNA 6mA in a replication-dependent but epigenetically independent manner.

To avoid possible confusion, here, misincorporated 6mA is named i6mA, postreplicative and methylase-deposited 6mA is named pr6mA, and 6mA is designated the collection of DNA i6mA and pr6mA. Chemically, i6mA has the same chemical structure as methylase-deposited pr6mA; thus, they are indistinguishable. Biophysically, like the truly methylated product pr6mA, misincorporated i6mA should also destabilize the DNA double helix,and thus ditto affects DNA replication and transcription and potentially falsify the epigenetic landscape of DNA pr6mA, which might be present at extremely low abundance[13,42]. Collectively, i6mA, which is unintentionally set on DNA, should be considered a form of DNA damage.

In this work, by taking advantage of unique heavy stable isotope tracing, we examined the misincorporation of DNA i6mA in response to intracellular RNA m6A degradation. We found that intracellular RNA m6A degradation cannot induce any i6mA. Furthermore, we discovered a deaminase ADAL-pivoted and adenylate kinase 1 (AK1)-assisted catabolism checkpoint. Mechanistically, the identified checkpoint blocks the reformulation of RNA decay-derived m6A nucleotides into 6mdATP and thus eliminates misincorporated i6mA in the process of intracellular RNA m6A degradation followed by purine salvaging.

Results

Labeling of RNA m6A by heavy stable isotope-labeled adenine nucleoside

We first exploited heavy stable isotope-labeled nucleoside [$^{15}N_5$]-adenosine ([$^{15}N_5$]-rA) to trace the catabolism of RNA m6A. We treated mouse embryonic stem (mES) cells with [$^{15}N_5$]-rA (Fig. 1A) and applied highly sensitive ultrahigh-performance liquid chromatography-tandem mass spectrometry (UHPLC-MS/MS) to detect the labeling of RNA in the [$^{15}N_5$]-rA-treated mES cells. As revealed by UHPLC-MS/MS analysis, mRNA adenosine (rA) was substantially labeled by nitrogen-15 (^{15}N) atoms (~ 62.5% of the total rA bases, Fig. 1B & 1C). Notably, the labeled rA was present in two forms, [$^{15}N_4$]-rA and [$^{15}N_5$]-rA (Fig. 1B & 1C). The observation of a major form [$^{15}N_4$]-rA suggested that the labeling reagent [$^{15}N_5$]-rA underwent deamination by adenine deaminase (Ada) followed by reamination via the purine salvage pathway (Fig. S1A). This process is similar to that of [$^{15}N_5$]-2'-deoxyadenosine (dA) labeling as reported recently[43]. mRNA m6A was also efficiently labeled (~ 60% of the total m6A bases) and consistently present in two forms, major [$^{15}N_4$]-m6A and minor [$^{15}N_5$]-m6A.

Intracellular RNA m6A degradation cannot induce misincorporated DNA i6mA

Recently, it was reported that intracellular RNA m6A degradation could induce misincorporated DNA i6mA in a number of cells, including mES cells and HEK293T cells[41]. As noted, the misincorporation of i6mA showed a delayed phase (~ 5 days delay) compared to de novo RNA synthesis[41]. Following this clue, we treated mES cells with the tracer [$^{15}N_5$]-rA over 7 days. With a high labeling efficiency (60%), the labeled mRNA m6A reached a level of 2.26 per 10^3 rC (Fig. 1C), but no labeled 6mA ([$^{15}N_4$]-6mA and [$^{15}N_5$]-6mA) was detected, except trace amounts of the unlabeled 6mA in genomic DNA (8.8 per 10^8 dC) (Fig. 1C). Even after 50 days of labeling for tracing RNA m6A degradation, we still failed to observe any labeled 6mA in the genomic DNA of mES cells (Fig. 1D, upper panel). After performing similar treatments (7–50 days), we did not observe any labeled 6mA in HEK293T cells yet (Fig. 1D, lower panel). Notably, our UHPLC-MS/MS method could detect 6mA with a sensitivity of less than one 6mA per 10^8 total dA. These results consistently support that intracellular RNA m6A degradation cannot induce any misincorporated DNA 6mA.

We also treated mES cells with a second heavy stable isotope tracer, [D_3]-L-methionine, for 7 days. *In vivo*, the tracer [D_3]-L-methionine is transformed into the methyl donor [D_3]-S-adenosyl-L-methionine ([D_3]-SAM) by SAM synthetase, and the latter is utilized by diverse methylases as a methyl donor to modify nucleic acid bases (Fig. S1B). To verify this probability, we first detected [D_3]-5-methyl-2'-deoxycytidine ([D_3]-5mC) in DNA and [D_3]-5-methylcytidine ([D_3]-m5C) in mRNA. We observed similar labeling ratios of > 80% for both [D_3]-5mC and [D_3]-m5C (Fig. S1C & S1D), proving that [D_3]-L-methionine was effectively converted into the methyl donor [D_3]-SAM. Consistently, we detected abundant mRNA [D_3]-m6A with a labeling efficiency of 90% (Fig. 1E & 1F) in [D_3]-L-methionine-treated mES cells;

however, no [D_3]-6mA was detected in genomic DNA, although trace amounts of unlabeled 6mA were detected (3.7 per 10^8 dC) (Fig. 1E & 1F).

The above data consistently supported the absence of labeled DNA 6mA no matter intracellular RNA m6A was labeled with [$^{15}N_4$] or [D_3]. These results drove us to propose the existence of a catabolic RNA m6A checkpoint that blocks the reformulation of intracellular RNA m6A degradation products to form incorporable 6mdATP and thus eliminates DNA 6mA misincorporation.

The deaminase ADAL preferentially catabolize 6mdAMP *in vitro*

Previous studies have shown that the adenine deaminase-like protein ADAL can protect RNA by reducing m6A misincorporation[44]. However, it is not known whether ADAL can suppress DNA misincorporation. We speculated that ADAL might catabolize N^6-methyldeoxyadenosine monophosphate (6mdAMP) to nontoxic deoxyinosine monophosphate (dIMP) (Fig. 2A). If so, ADAL should play a critical role in the catabolism checkpoint blocking i6mA misincorporation. This drove us to test the catalytic activity of ADAL on 6mdAMP. We first investigated the activity of mouse recombinant ADAL protein on m6AMP. As detected by UHPLC-MS/MS analysis, the recombinant ADAL protein catabolized m6AMP to inosine monophosphate (rIMP) (Fig. 2B). The result is in agreement with previous report[44,45]. Then, we investigated the catalytic activity of mouse recombinant ADAL protein on 6mdAMP *in vitro*. Interestingly, the recombinant ADAL protein also catabolized 6mdAMP to dIMP (Fig. 2C). Along with reductions in 6mdAMP (detected in the form of 6mA by UHPLC-MS/MS), a dramatic increase in the level of the nontoxic product dIMP (detected in the form of dI) was observed (Fig. 2C). Evidently, ADAL displays a novel ability to catalyze the deamination of 6mAMP nucleotides *in vitro*.

To further explore the relative catalytic activity, we next measured the catalytic efficiency (K_{cat}/K_m) of ADAL for both 6mdAMP and m6AMP. As shown in Fig. 2D, in our *in vitro* reaction system, the catalytic efficiency of ADAL for 6mdAMP was 33.4 ± 0.83 mM^{-1} s^{-1}. This value is 2.14 fold as high as that of ADAL for m6AMP (15.6 ± 0.71 mM^{-1} s^{-1}) (Fig. 2E). In addition, the ADAL protein showed greatly reduced activity toward 6mA deoxynucleoside and 6mdATP (Fig. S2A & S2B). These data support that ADAL preferentially catabolizes 6mdAMP.

The deaminase ADAL functions as the key checkpoint enzyme *in vivo*

To determine the roles of ADAL in the catabolism checkpoint *in vivo*, we knocked down *Adal* mRNA in mES cells via small interfering (si) RNA transfection (Fig. 3A). As revealed by sensitive UHPLC-MS/MS analysis, both [$^{15}N_4$]-6mA and [$^{15}N_5$]-6mA were indeed detected in the genomic DNA of *Adal* siRNA (si*Adal*)-transfected cells (Fig. 3B). To further verify this effect, we used clustered regularly interspaced short palindromic repeat/CRISPR-associated protein 9 (CRISPR/Cas9)-mediated nonhomologous end joining (NHEJ) for generating *Adal*-deficient mES cells (*Adal*$^{-/-}$) (Fig. 3C). The gene sequencing results confirmed the successful knockout of the *Adal* gene in *Adal*$^{-/-}$ mES cells (Fig. 3C). After the treatment with [$^{15}N_5$]-rA for 7 days, the *Adal*$^{-/-}$-1 and *Adal*$^{-/-}$-2 mES cells also exhibited detectable [$^{15}N_4$]-6mA and [$^{15}N_5$]-6mA in their genomic DNA (Fig. 3D). The levels of [$^{15}N_4$]-6mA and [$^{15}N_5$]-6mA are on average approximately 5.9 per 10^8 dC and 3.2 per 10^8 dC (Fig. 3D), respectively. Consistently, without the depletion of ADAL, no labeled 6mA was detected in the negative control siRNA (siCTRL)-transfected mES cells (Fig. 3B) and in the knockout-absent wild-type mES cells (Fig. 3D).

To explore the impacts of other deamination reactions on the DNA 6mA misincorporation, we further inhibited AMP deaminase and adenine deaminase (Ada) using the inhibitors cpd3 ((S)-6-(4-(((1-(isoquinolin-8-yl) ethyl) amino)

methyl) phenyl) nicotinic acid) and DCF (2'-deoxycoformycin), respectively. The AMP deaminase inhibitor cpd3 could not reduce the level of RNA [$^{15}N_4$]-m6A (Fig. S3A) and failed to induce any misincorporated 6mA (indicated by the labeled 6mA) (Fig. S3B). Treatment with DCF (0.1 ~ 100 μM) significantly increased the level of RNA [$^{15}N_5$]-m6A and concomitantly reduced the levels of [$^{15}N_4$]-m6A and unlabeled m6A (Fig. S3C). However, no labeled 6mA was detected in the genomic DNA of mES cells that were treated with DCF (Fig. S3D).

The m6A demethylases FTO and ALKBH5 can erase the methyl group of mRNA m6A [46,47] and downregulate the level of mRNA m6A. Surprisingly, the depletion of these enzymes (by CRISPR/Cas9-based knockout) also failed to induce any labeled 6mA in genomic DNA (Fig. S3E and S3F).

These results support that only the deaminase ADAL is critically involved in the checkpoint for suppressing 6mA misincorporation and that other known adenine-related deaminases and m6A demethylases do not have any direct role in this checkpoint.

Adenylate kinase 1 is an important accessary factor maintaining the catabolic checkpoint

To further identify the factors involved in the checkpoint, we constructed a series of overexpression plasmids for nucleotide kinases functioning in the purine salvage synthesis pathway, including adenosine kinase (ADK), adenine phosphoribosyltransferase (APRT), adenylate kinase 1 (AK1*)*, and adenosine diphosphate kinase (DNPK). These proteins are hypothesized to facilitate the formation of 6mdATP by increasing phosphorylation at a certain step in the purine salvage pathway. However, no labeled 6mA was detected in any of the gene overexpression groups or control groups of wild-type mES cells (Fig. S4). These results may suggest that such a simple increase in the expression of nucleotide kinases cannot break the misincorporation-suppressing checkpoint. Then, we replaced wild-type cells with *Adal*$^{-/-}$ cells to explore whether nucleotide kinases are regulatory factors rather than determining factors for the checkpoint. As shown in Fig. 4, notably, the level of labeled 6mA in the *AK1*-overexpressing group (7.80 per 10^7 dC) is approximately 3.25-fold higher than that in the control group (EV, 2.40 per 10^7 dC). In contrast, the labeled 6mA level in the *ADK*-, *APRT*-, and *NDPK*-overexpressing groups (1.94–2.29 per 10^7 dC) is similar to that in the control group. These results suggest that AK1 participates in the catabolism checkpoint of RNA m6A.

Preferential misincorporation of m6A in RNA revealed by extracellular m6A treatment

Our unpublished data showed that m6A nucleosides could be detected in human urine at a high abundance, indicating the presence of nonnegligible extracellular m6A-related species in humans. Therefore, in addition to intracellular RNA m6A degradation, humans may be exposed to extracellular m6A-related nucleosides or nucleotides. To test the effects of such exposure, we exploited the heavy stable isotope tracer [D_3]-m6A nucleoside to examine extracellular m6A-induced misincorporation. After treatment with [D_3]-m6A nucleoside (0.2–1.0 μM), RNA [D_3]-m6A was detected in both wild-type mES and *Adal*$^{-/-}$ cells (Fig. 5A, S5A). The levels of RNA [D_3]-m6A and DNA [D_3]-6mA in *Adal*$^{-/-}$ cells were 17 ~ 44- and 17 ~ 303-fold higher than those in wild-type cells, respectively (Fig. S5A, S5B). Notably, after treatment with 0.1 μM [D_3]-m6A nucleoside, neither RNA [D_3]-m6A nor DNA [D_3]-6mA was detected in the wild-type cells. However, under treatment with this low dose (0.1 μM [D_3]-m6A), the depletion of *Adal* dramatically increased the levels of RNA [D_3]-m6A and DNA [D_3]-6mA (Fig. 5B & Fig. S5A and S5B). These results together suggest that ADAL can catabolize 6mdAMP in a dose-dependent manner and remove all 6mdAMP generated from m6A nucleoside at a concentration of ≤ 0.1 μM.

In addition, the levels of RNA [D_3]-m6A and DNA [D_3]-6mA in *Adal*$^{-/-}$ cells increased with increasing concentrations of [D_3]-m6A nucleoside (Fig. 5B). By linear regression of the incorporation level with the treatment dose (0.2–1.0 μM),

the values of the slopes for RNA [D_3]-m6A and DNA [D_3]-6mA were estimated to be approximately 3241.5 and 357.5 (Fig. 5B), respectively. These values suggested that RNA m6A misincorporation is 9.1-fold as high as DNA 6mA misincorporation, supporting a preference on RNA misincorporation.

Differential ADAL expression in cancers

We also analyzed the potential clinical significance of ADAL in four human cancers based on the TCGA data sets. In cervical squamous cell carcinoma, kidney renal papillary carcinoma, pancreatic ductal adenocarcinoma, and rectum adenocarcinoma, patients with low ADAL expression in tumor tissues had worse survival rates than those with high ADAL expression (Fig. 6). This hints that the ADAL aberrance may play a critical role in cancer development.

Discussion

Unique Ada deamination-mediated [$^{15}N_5$]-rA labeling. In this work, one heavy stable isotope-labeling strategy involved the use of the nucleoside [$^{15}N_5$]-rA. [$^{15}N_5$]-rA could be utilized for RNA synthesis, as indicated by the observation of [$^{15}N_5$]-rA in RNA. Interestingly, in addition to RNA [$^{15}N_5$]-rA, we also observed a new but major form, [$^{15}N_4$]-rA, in RNA. Likely, the presence of RNA [$^{15}N_4$]-rA should be associated with the deamination activity of Ada. Indeed, after inhibiting Ada activity using the specific inhibitor DCF, we observed an increase in RNA [$^{15}N_5$]-rA (data not shown). The observations support that the formation of [$^{15}N_4$]-rA is associated with the deamination activity of Ada. Essentially, we showed an Ada deamination-mediated labeling strategy that is unique for Ada-containing mammalian cells.

Noteworthy, in [$^{15}N_5$]-rA-treated cells, we observed efficient labeling of mRNA m6A, too. Consistent with the observation of the two forms of labeled rA ([$^{15}N_4$]- and [$^{15}N_5$]-rA) in RNA, we also observed two forms of labeled RNA m6A ([$^{15}N_4$]- and [$^{15}N_5$]-m6A). Upon Ada inhibition, we observed an increase in [$^{15}N_5$]-m6A and a concomitant decrease in [$^{15}N_4$]-m6A (Fig. S3C). As the METTL3/METTL14 methyltransferase complex is solely responsible for mediating the N^6-methylation of mRNA adenine[48], the labeled mRNA m6A should result from the methylation of [$^{15}N_4$]-rA and [$^{15}N_5$]-rA in mRNA by the METTL3/METTL14 complex. Indeed, upon the depletion of *Mettl3*, mRNA m6A lost, and we did not observe any labeled m6A in mRNA (data not shown). Taken together, intracellular RNA m6A can be traced using heavy stable isotope labeled rA.

Intracellular RNA m6A degradation cannot induce misincorporated DNA i6mA. By the use of the efficient [$^{15}N_5$]-rA labeling strategy, intracellular RNA m6A can be efficiently labeled. If the degraded RNA m6A could be reformulated to generate 6mdATP via purine salvage pathway, we should observe labeled DNA 6mA. However, we did not observe any labeled DNA 6mA over 7–50 days of treatment, indicating the absence of misincorporated DNA i6mA. Although it was reported that DNA misincorporation occurred at a delayed phase (approximately 5-day delay) in comparison to RNA labeling[41], our observation on the absence of labeled DNA 6mA (or misincorporated i6mA) over 50 days of treatment proves that the m6A nucleotides generated from RNA m6A decay are not reutilized in DNA replication. By the use of the second strategy involved [D_3]-L-methionine labeling, we also observed the labeled RNA m6A ([D_3]-m6A), but consistently did not observe any labeled DNA 6mA after 7 days of treatment. Notably, both labeling strategies showed high labeling efficiency (> 60%). Collectively, our data strongly support that intracellular RNA m6A decay cannot induce any misincorporated DNA i6mA at least in the tested cells.

Checkpoint, ADAL, and AK1. Given the capacity of DNA polymerases to incorporate 6mdATP[13] and the absence of the labeled DNA 6mA (also misincorporated i6mA herein), we infer that the degradation products of RNA m6A cannot be

ultimately converted into 6mdATP via the purine salvage pathway. This inference drives us to propose that a checkpoint functioning similar to that in the cell cycle[49,50] and in the immunological response[51–53] exists for suppressing DNA misincorporation along with RNA m6A degradation. Essentially, we identified two players in this proposed checkpoint, ADAL and AK1.

The depletion of the deaminase *Adal* by either knockdown or knockout resulted in the presence of the labeled DNA 6mA. In contrast, the depletion of the mRNA m6A demethylase FTO or ALKBH5 did not break the checkpoint, nor did overexpression of the kinases involved in the purine salvage pathway alone. All these findings support the idea that ADAL plays a pivotal role in the checkpoint. Mechanistically, ADAL simultaneously catabolizes the methylated nucleotides m6AMP and 6mdAMP to the nontoxic nucleotides IMP and dIMP, respectively, reducing the misincorporation of N^6-methyladenine via DNA polymerase; thus, the hydrolysis of both m6AMP and 6mdAMP by ADAL contributes critically to the blockade of replication-dependent 6mA incorporation. Moreover, the catabolizing activity of ADAL toward 6mdAMP is 2.14-fold as high as that toward m6AMP. Of note, here we showed, for the first time, the activity of ADAL in catabolizing 6mdAMP. Collectively, our data indicate that ADAL functions as a key checkpoint enzyme to block the catabolic conversion of intracellular RNA m6A to genomic DNA 6mA by catabolizing both m6AMP and 6mdAMP, particularly the latter.

In addition to the deaminase ADAL, adenylate kinase 1 (AK1) was identified as a protein involved in the checkpoint. Overexpression of AK1 did not induce any detectable labeling of DNA i6mA in the presence of sufficient ADAL but increased the labeled DNA i6mA in the absence of ADAL. This finding suggests that the phosphorylation of 6mdAMP into 6mdADP is a much slower process than the hydrolysis of 6mdAMP mediated by ADAL. In other words, the preferential substrate for AK1 is not 6mdAMP but dAMP, which is required for DNA synthesis. Overexpression of AK1 can partially compensate for the slow phosphorylation of 6mdAMP by AK1. The slow phosphorylation process would provide a time window long enough for ADAL to catabolize the generated 6mdAMP completely.

Source of the unlabeled DNA 6mA. As shown in this work, in mES cells treated with heavy stable isotope tracers, we found large proportions of the labeled m6A in both mRNA and total RNA, but no labeled genomic 6mA was detected. However, trace amounts of the unlabeled 6mA were detected. This finding is consistent with our recent work[13]. The observed unlabeled DNA 6mA was formed through polymerase-dependent misincorporation[13,41]. However, the source for generating the unlabeled 6mA was not known yet. In this work, we clearly showed that the observed DNA 6mA did not originate from intracellular RNA m6A, as described above. Because more than three-quarters of the m6A modifications were labeled, it is impossible that only unlabeled RNA m6A was incorporated into genomic DNA, and the labeled m6A could not be incorporated via the purine salvage pathway. The absence of the labeled DNA 6mA also excludes an origin from methylase-deposited methylation. We speculate that the observed DNA i6mA originated from catabolism of extracellular RNA m6A. Indeed, we detected urinary m6A nucleosides at high abundance (data not published), suggesting the existence of free m6A in extracellular spaces in humans. Meanwhile, by the extracellular exposure of heavy stable isotope-labeled m6A nucleoside, we clearly showed that exogenous m6A nucleoside can induce misincorporated DNA 6mA and such a process is also restricted by ADAL-pivoted checkpoint. It is reasonable that, under physiological conditions, both intracellular and extracellular RNA m6A are tightly regulated by the catabolism checkpoint. Biochemically, the N^6-methyladenine modification on the DNA template disturbs base pairing[54,55], hinders new chain extension, affects replication[24] and transcription[23], and regulates related gene expression[22,54]. Therefore, a strict catabolism checkpoint of N^6-methyladenine is required to maintain genome integrity.

Biological implications. The expression of ADAL varies in different cells. It is expected that misincorporated i6mA could be observed in cells that express ADAL at low levels. Musheev et al[41] reported that C2C12 and especially NIH 3T3 cells had exceptionally high levels of misincorporated i6mA, 13–500 i6mA per million dA. However, by our experiments on C2C12 and NIH 3T3 cells, we observed i6mA at a level of 100 folds lower (Fig. S6). We did not detect misincorporated i6mA in 293T and mES cells. Collectively, the misincorporated i6mA must be strictly controlled.

Our observation on the blockade of DNA 6mA misincorporation strongly suggests that the epigenetic DNA 6mA landscape should be tightly maintained in the tested cells. Essentially, the findings on epigenetic mark DNA 6mA remain elusive due to the neck-of-bottle of analytical technologies for 6mA detection, the contamination of coexisting bacteria carrying abundant 6mA, poor LC-MS/MS skill, and a lack of reliable 6mA sequencing technology[56]. However, it is still very surprising that misincorporated i6mA must be strictly controlled, while epigenetic pr6mA is rarely found in human cells. These conflicting observations may hint that true epigenetic 6mA (methylase-deposited 6mA) should have extremely important functions and appear in every cell in certain scenarios, e.g., responses to certain stimuli. Otherwise, the mammalian cells should not set such a strict bar for misincorporation. Interestingly, as the most important and abundant epigenetic mark, misincorporation of 5mC must also be strictly controlled[57–59]. In contrast, DNA 5-hydroxymethylcytosine (5hmC) is found only in limited cells at moderate abundance and can be misincorporated into genomic DNA[60]. On the other hand, low expression of *Adal* may shorten the survival of cancer patients (Fig. 6). These data and underlying logics allow us to infer that the ADAL-pivoted checkpoint and the suppression of i6mA misincorporation have biological importance, at least in tumor development and therapy.

RNA m6A checkpoint in the purine salvage pathway. In the free nucleotide pool, free m6AMP can be recycled by rephosphorylation via nucleotide kinases and further reduced to N^6-methyldeoxyadenosine diphosphate (6mdADP) by ribonucleotide reductase. 6mdADP is next transformed into 6mdATP, which is utilized by DNA polymerases, forming DNA i6mA. Our results indicated that the substantially labeled RNA m6A in mES cells was not transformed and incorporated into genomic DNA. Taken together, our findings led us to propose a catabolic checkpoint of N^6-methyladenine along with the purine pathway (Fig. S7). This checkpoint functions to block potential DNA 6mA misincorporation via ADAL-mediated hydrolysis of both m6AMP and 6mdAMP, AK1 mediated restriction on the phosphorylation of 6mdAMP, and other unknown steps.

In this work, by exploiting unique heavy stable isotope labeling technology coupled with sensitive UHPLC-MS/MS analysis, we demonstrated that ADAL catabolizes m6AMP and, more efficiently, 6mdAMP to nontoxic nucleotides and blocks DNA 6mA misincorporation. In addition, adenylate kinase 1 also contributes to the suppression of DNA 6mA misincorporation by limiting the rate of 6mdAMP phosphorylation, which may provide adequate time for ADAL to catabolize 6mdAMP. Therefore, ADAL and AK1 together suppress DNA 6mA misincorporation and maintain genomic epigenetic integrity.

Materials And Methods

Reagents and material

[$^{15}N_5$]-adenosine ([$^{15}N_5$]-rA), [$^{15}N_3$]-deoxycytidine ([$^{15}N_3$]-dC), [$^{15}N_3$]-cytidine ([$^{15}N_3$]-rC) and [D_3]-L-methionine were ordered from Cambridge Isotope Laboratories Inc. (Andover, MA, USA). 2'-deoxyadenosine (dA), adenosine (rA), 2'-deoxycytidine (dC), cytidine (rC), N^6-methyl-2’-deoxyadenosine (6mA), N^6-methyladenosine (m6A), 5-methyl-2’-deoxycytidine (5mC), 5-methylcytidine (m5C), phosphodiesterase I (SVP), nuclease P1 (NP1), cpd3 ((S)-6-(4-(((1-(isoquinolin-8-yl)ethyl)amino)methyl)phenyl)nicotinic acid) and DCF (2’-deoxycoformycin) were purchased from

Sigma-Aldrich Inc. (St. Louis, MO, USA). Benzonase was purchased from Sino Biological Inc. (Beijing, China). Calf intestinal alkaline phosphatase (CIP) was ordered from New England Biolabs Inc. (Ipswich, MA, USA). TRIzol reagent was purchased from Thermo Fisher Scientific Inc. (Waltham, MA, USA). Anti-FTO (ab92821) and anti-ALKBH5 (ab195377) antibodies were purchased from Abcam Inc. (Cambridge, UK). The secondary antibodies goat anti-rabbit IgG (H + L) DyLight 800 and goat anti-mouse IgG (H + L) DyLight 800 were purchased from Bioworld Technology, Inc. (St. Louis Park, MN, USA). [D_3]-N^6-methyladenosine ([D_3]-m6A) was purchased from Toronto Research Chemicals (North York, Canada).

Cell culture and stable isotope tracers label

mES cells (129SvEv) were cultured in high-glucose DMEM (Thermo) supplemented with 15% fetal bovine serum (Thermo), 0.35% penicillin-streptomycin solution (Thermo), 1000 U/ml mouse leukemia inhibitory factor (mLIF) (Millipore, Germany), 100 μM β-mercaptoethanol, 3.0 μM Stemolecule CHIR99021 (Stemgent, USA), 1 μM Stemolecule PD0325901 (Stemgent), 100 μM nonessential amino acids (Thermo), 2 mM L-glutamine (Thermo), and 1 mM sodium pyruvate (Thermo). The mES cells were confirmed to be free of mycoplasma contamination and were incubated at 37°C in a bacteria-free incubator with 5% CO_2. The mES cell culture dishes were coated with 0.1% sterilized gelatin aqueous solution before use.

To be labeled with stable isotope tracers [$^{15}N_5$-rA] or [D_3]-L-methionine, mES cells were seeded into gelatin-coated 6-well cell culture clusters at a density of 10^5 per well. Then, 20 μM [$^{15}N_5$]-rA or 30 μg/ml [D_3]-L-methionine was added to the culture medium, and the medium was replaced with fresh medium containing [$^{15}N_5$]-rA or [D_3]-L-methionine every 24 h. This treatment was performed over 7 days.

DNA extraction and enzymolysis

mES cells to be analyzed were harvested and collected into 1.5 ml aseptic centrifuge tubes. Then, genomic DNA was extracted using a Promega Wizard® Genomic DNA Purification Kit (Promega, USA) according to the manufacturer's instructions. Contamination was avoided as much as possible during DNA extraction. The newly extracted DNA was quantitated using a NanoDrop 2000 (Thermo).

Before UHPLC-MS/MS analysis, 5.0 μg of DNA was dissolved in 50 μl of enzymatic digestion buffer (10 mM Tris-HCl (pH 8.0) and 1 mM Mg^{2+}) and then digested to 2'-deoxynucleosides with an enzyme mixture of 1 U of benzonase, 0.02 U of SVP, and 1 U of CIP at 37°C for 12 h. Next, the enzymes were removed by ultrafiltration (molecular weight cutoff: 3 kDa; Pall Corporation, USA). The filtered solution containing 2'-deoxynucleosides was subjected to UHPLC-MS/MS analysis.

RNA (and mRNA) extraction and enzymolysis

Total RNA was extracted with TRIzol Reagent (Thermo) according to the manufacturer's instructions. mES cells were harvested and collected into 1.5 ml aseptic centrifuge tubes on ice. Then, the cell pellets were lysed and homogenized in TRIzol reagent and immediately subjected to chloroform extraction and ethanol precipitation. The extracted total RNA was dissolved in DEPC-treated water and quantitated using a NanoDrop 2000 (Thermo). Then, mRNA was extracted from the total RNA using a Dynabeads™ mRNA Purification Kit (Thermo) according to the manufacturer's instructions.

Enzymatic digestion of RNA (5.0 μg) was conducted with a mixture of 1 U of benzonase, 0.25 U of NP1, 0.02 U of SVP, and 1 U of CIP in Tris-HCl buffer (10 mM Tris-HCl, pH 8.0, plus 1 mM Mg^{2+}) at 37°C for 12 h. Then, the enzymes were removed by ultrafiltration (molecular weight cutoff: 3 kDa; Pall Corporation, USA). The filtered solution containing nucleosides was subjected to UHPLC-MS/MS analysis.

siRNA transfection

mES cells were seeded into 6-well cell culture clusters at a density of 10^5 per well the night before transfection with 30 pmol of siRNA against Adal using Lipofectamine RNAiMAX Transfection Reagent (Thermo) according to the manufacturer's protocols. Control cells were transfected with 30 pmol of negative control sequence. The transfected mES cells were cultured for another 36 h before qPCR analysis or 48 h before western blot analysis.

UHPLC-MS/MS analysis

UHPLC-MS/MS analysis was performed as described previously[13]. Enzymatic digestion products of DNA and RNA were injected into an Agilent 1290 II UHPLC system coupled with an electrospray ionization (ESI)-triple quadrupole mass spectrometer (6470, Agilent Technologies, Santa Clara, CA), and a Zorbax SB-Aq column (2.1 × 100 mm, 1.8 μm particle size, Agilent, USA) was used for separation. The mass spectrometer was operated under positive ionization using multiple reaction monitoring (MRM) mode.

The selective MRM transitions for DNA 2'-deoxynucleoside analysis were as follows:

dA: m/z 252→136, [$^{15}N_4$]-dA: m/z 256→140, [$^{15}N_5$]-dA: m/z 257→141, dC: m/z 228→112, [$^{15}N_3$]-dC: m/z 231→115, 5mdC: m/z 242→126, [D_3]-5mdC: m/z 252→136, 6mA: m/z 266→150, [D_3]-6mA: m/z 269→153, [$^{15}N_4$]-6mA: m/z 270→154, and [$^{15}N_5$]-6mA: m/z 271→151.

Those for RNA nucleoside analysis were as follows:

rA: m/z 268→136, [$^{15}N_4$]-rA: m/z 272→140, [$^{15}N_5$]-rA: m/z 273→141, rC: m/z 244→112, [$^{15}N_3$]-rC: m/z 247→115, m5C: m/z 258→126, [D_3]-m5C: m/z 261→136, m6A: m/z 282→150, [D_3]-m6A: m/z 285→153, [$^{15}N_4$]-m6A: m/z 286→154, and [$^{15}N_5$]-6mA: m/z 287→154. The fragmentation voltage for all the MRM transitions was set at 90 V, and the nebulization gas pressure was set at 40 psi. The other conditions were as described previously[13].

Treatment of mES cells with extracellular m6A nucleotides

mES cells of wild-type or *Ada1*$^{-/-}$ were seeded into 6-well cell culture clusters at a density of 2×10^5 per well, and fresh cell culture medium was supplemented with [D_3]-m6A nucleoside at concentrations of 0, 0.1, 0.2, 0.5, or 1 μM. The treated cells were harvested after incubation for 2 days, and DNA and RNA were extracted for further analysis.

Activity analysis of ADAL *in vitro*

An ADAL fusion protein whose N-terminus was tagged with maltose-binding protein (MBP) was expressed in *E. coli* and then purified via a prepacked hydrophobic interaction chromatography column and a prepacked MBP-Trap HP 5 ml column (GE Healthcare, Uppsala, Sweden). Then, the purity was analyzed with a BCA Protein Assay Kit (Beyotime) and via SDS polyacrylamide gel electrophoresis (PAGE).

Next, we prepared 6mdAMP by digesting plasmid DNA that carries abundant DNA 6mA. The plasmid DNA was extracted from E. coli. The plasmid of 10 μg was digested in a 100 μl reaction mixture containing 10 mM Tris-HCl (pH 8.0), 2 mM Mg^{2+}, 1 U of benzonase, and 0.02 U of SVP. After 6 h of incubation, the mixture was filtrated by centrifugation through an ultrafiltration tube (MW cutoff: 3 kDa; Pall Corporation, USA). Then, the filtrated solution was mixed with 400 nM m6AMP. By this protocol, solutions containing two ADAL substrates, 6mdAMP and m6AMP, were prepared. For characterization of the preparations, 1.5 μg product that had been treated with 1.0 U CIP for 1 h, and an equivalent amount of untreated product was analyzed by UHPLC-MS/MS for quantification of 6mA or m6A.

The difference in 6mA or m6A between the CIP-treated product and the untreated product represented the content of monophosphorylated N^6-methyladenine.

An ADAL activity assay was conducted in 50 μl reaction buffer (20 mM Tris-HCl (pH 7.0), 0.1 μg/μl BSA, 2 mM DTT) supplemented with 1.5 μg of the above enzymatic products containing m6AMP andr 6mAMP and 0 or 0.5 μg of ADAL protein at 37°C for 1 h. After the reactions, the solutions were treated with proteinase K at 55°C for 30 min and heated for enzyme inactivation at 95°C for 10 min and then incubated with 5.0 U CIP for another 1 h. The reaction substrates m6AMP and 6mAMP and the products rIMP and dIMP were converted into m6A, 6mA, rI, and dI, respectively, for UHPLC-MS/MS analysis. After passing through ultrafiltration tubes (MW cutoff: 3 kDa), the nucleoside solution was subjected to UHPLC-MS/MS analysis.

The catalytic efficiency (K_{cat}/K_m) of ADAL for m6AMP and 6mAMP was analyzed in a 50 μl reaction mixture of 20 mM Tris-HCl (pH 7.0), 0.1 μg/μl BSA, 2 mM DTT, 0.2 μg of ADAL protein, and varying concentrations of the test compound. After incubation at 37°C for 10 min, the reaction mixture was incubated with 5.0 U of CIP for another 1 h to convert all of the nucleotides in the mixture into nucleosides.

Declarations

Acknowledgments

Funding: This work is supported by the National Natural Science Foundation of China [21927807, 91743201, and 22021003], and Sanming Project of Medicine in Shenzhen [No. SZM201811070].

Data and materials availability:

All data needed to evaluate the conclusions in the paper are present in the paper and/or the Supplementary Materials. Additional data related to this paper may be requested from the authors.

References

1. Messer, W. & Noyer-Weidner, M. Timing and targeting: the biological functions of Dam methylation in E. coli. *Cell* **54**, 735-737 (1988).
2. Wion, D. & Casadesús, J. N^6-methyl-adenine: an epigenetic signal for DNA–protein interactions. *Rev. Microbiol.* **4**, 183-192 (2006).
3. Fang, G. et al. Genome-wide mapping of methylated adenine residues in pathogenic Escherichia coli using single-molecule real-time sequencing. *Biotechnol.* **30**, 1232-1239 (2012).
4. Vanyushin, B., Belozersky, A., Kokurina, N. & Kadirova, D. 5-methylcytosine and 6-methylaminopurine in bacterial DNA. *Nature* **218**, 1066-1067 (1968).
5. Fu, Y. et al. N^6-methyldeoxyadenosine marks active transcription start sites in Chlamydomonas. *Cell* **161**, 879-892 (2015).
6. Beh, L. Y. et al. Identification of a DNA N6-adenine methyltransferase complex and its impact on chromatin organization. *Cell* **177**, 1781-1796. e25 (2019).
7. Mondo, S. J. et al. Widespread adenine N6-methylation of active genes in fungi. *Genet.* **49**, 964-968 (2017).
8. Greer, E. L. et al. DNA methylation on N^6-adenine in C. elegans. *Cell* **161**, 868-878 (2015).
9. Zhang, G. et al. N^6-methyladenine DNA modification in Drosophila. *Cell* **161**, 893-906 (2015).

10. Liang, Z. et al. DNA N^6-adenine methylation in Arabidopsis thaliana. *Cell* **45**, 406-416. e3 (2018).
11. Zhou, C. et al. Identification and analysis of adenine N^6-methylation sites in the rice genome. *Plants* **4**, 554-563 (2018).
12. Liu, J. et al. Abundant DNA 6mA methylation during early embryogenesis of zebrafish and pig. *Commun.* **7**, 13052 (2016).
13. Liu, X. et al. N^6-methyladenine is incorporated into mammalian genome by DNA polymerase. *Cell Res.* **31**, 94-97 (2021).
14. Yao, B. et al. DNA N6-methyladenine is dynamically regulated in the mouse brain following environmental stress. *Nature Commun.* **8**, 1122 (2017).
15. Xiao, C. L. et al. N^6-methyladenine DNA modification in the human genome. *Cell* **71**, 306-318. e7 (2018).
16. Wu, T. P. et al. DNA methylation on N^6-adenine in mammalian embryonic stem cells. *Nature* **532**, 329-333 (2016).
17. Wang, Y., Chen, X., Sheng, Y., Liu, Y. & Gao, S. N^6-adenine DNA methylation is associated with the linker DNA of H2A. Z-containing well-positioned nucleosomes in Pol II-transcribed genes in Tetrahymena. *Nucleic Acids Res.* **45**, 11594-11606 (2017).
18. Luo, G. Z. et al. N^6-methyldeoxyadenosine directs nucleosome positioning in Tetrahymena DNA. *Genome Biol.* **19**, 200 (2018).
19. Karrer, K. M. & Vannuland, T. A. Methylation of adenine in the nuclear DNA of Tetrahymena is internucleosomal and independent of histone H1. *Nucleic Acids Res.* **30**, 1364-1370 (2002).
20. Katz, D. J., Edwards, T. M., Reinke, V. & Kelly, W. G. A C. elegans LSD1 demethylase contributes to germline immortality by reprogramming epigenetic memory. *Cell* **137**, 308-320 (2009).
21. Luo, G. Z. & He, C. DNA N^6-methyladenine in metazoans: functional epigenetic mark or bystander? *Struct. Mol. Biol.* **24**, 503-506 (2017).
22. Ma, C. et al. N6-methyldeoxyadenine is a transgenerational epigenetic signal for mitochondrial stress adaptation. *Cell Biol.* **21**, 319-327 (2019).
23. Wang, W. et al. Epigenetic DNA modification N^6-methyladenine causes site-specific RNA polymerase II transcriptional pausing. *Am. Chem. Soc.* **139**, 14436-14442 (2017).
24. Li, B. et al. Epigenetic DNA modification N^6-methyladenine inhibits DNA replication by DNA polymerase of Pseudomonas aeruginosa Phage PaP1. *Res. Toxicol.* **32**, 840-849 (2019).
25. Wei, C. M., Gershowitz, A. & Moss, B. Methylated nucleotides block 5′ terminus of HeLa cell messenger RNA. *Cell* **4**, 379-386 (1975).
26. Meyer, K. D. et al. Comprehensive analysis of mRNA methylation reveals enrichment in 3' UTRs and near stop codons. *Cell* **149**, 1635-1646 (2012).
27. Dominissini, D. et al. Topology of the human and mouse m6A RNA methylomes revealed by m6A-seq. *Nature* **485**, 201-206 (2012).
28. Nachtergaele, S. & He, C. The emerging biology of RNA post-transcriptional modifications. *RNA Biol.* **14**, 156-163 (2017).
29. Roundtree, I. A., Evans, M. E., Pan, T. & He, C. Dynamic RNA modifications in gene expression regulation. *Cell* **169**, 1187-1200 (2017).
30. Yang, Y. et al. Dynamic m^6A modification and its emerging regulatory role in mRNA splicing. *Bull.* **60**, 21-32 (2015).

31. Zhao, B. S., Roundtree, I. A. & He, C. Post-transcriptional gene regulation by mRNA modifications. *Rev. Mol. Cell Biol.* **18**, 31-42 (2016).
32. Hambraeus, G., Von Wachenfeldt, C. & Hederstedt, L. Genome-wide survey of mRNA half-lives in Bacillus subtilis identifies extremely stable mRNAs. *Genet. Genom.* **269**, 706-714 (2003).
33. Sharova, L. V. et al. Database for mRNA half-life of 19977 genes obtained by DNA microarray analysis of pluripotent and differentiating mouse embryonic stem cells. *DNA Res.* **16**, 45-58 (2009).
34. Puckett, L., Chambers, S. & Darnell, J. E. Short-lived messenger RNA in HeLa cells and its impace on the kinetics of accumulation of cytoplasmic polyadenylate. *Natl. Acad. Sci. U.S.A.* **72**, 389-393 (1975).
35. Wang, Y. et al. Precision and functional specificity in mRNA decay. *Natl. Acad. Sci. U.S.A.* **99**, 5860-5865 (2002).
36. Houseley, J. & Tollervey, D. The many pathways of RNA degradation. *Cell* **136**, 763-776 (2009).
37. Valencia-Sanchez, M. A., Liu, J., Hannon, G. J. & Parker, R. Control of translation and mRNA degradation by miRNAs and siRNAs. *Genes Dev.* **20**, 515-524 (2006).
38. Sachs, A. B. Messenger RNA degradation in eukaryotes. *Cell* **74**, 413-421 (1993).
39. Nyhan, W. L. Nucleotide synthesis via salvage pathway. *In Encyclopedia of Life Sciences* (John Wiley & Sons, Ltd, 2001).
40. Jiang, H. P. et al. Modified nucleoside triphosphates exist in mammals. *Sci.* **9**, 4160-4167 (2018).
41. Musheev, M. U., Baumgartner, A., Krebs, L. & Niehrs, C. The origin of genomic N^6-methyl-deoxyadenosine in mammalian cells. *Chem. Biol.* **16**, 630-634 (2020).
42. Bochtler, M. & H. Fernandes. DNA adenine methylation in eukaryotes: Enzymatic mark or a form of DNA damage? *bioEssays* **43**, 2000243 (2021).
43. Liu, B., Liu, X., Lai, W. & Wang, H. Metabolically generated stable isotope-labeled deoxynucleoside code for tracing DNA N^6-methyladenine in human cells. *Chem.* **89**, 6202-6209 (2017).
44. Chen, M. et al. m^6A RNA degradation products are catabolized by an evolutionarily conserved N^6-methyl-AMP deaminase in plant and mammalian cells. *The Plant Cell* **30**, 1511-1522 (2018).
45. Murakami, E. et al. Adenosine deaminase-like protein 1 (ADAL1): characterization and substrate specificity in the hydrolysis of N^6- or O^6-substituted purine or 2-aminopurine nucleoside monophosphates. *Med. Chem.* **54**, 5902-5914 (2011).
46. Jia, G. et al. N6-methyladenosine in nuclear RNA is a major substrate of the obesity-associated FTO. *Chem. Biol.* **7**, 885-887 (2011).
47. Zheng, G. et al. ALKBH5 is a mammalian RNA demethylase that impacts RNA metabolism and mouse fertility. *Cell* **49**, 18-29 (2013).
48. Liu, J. et al. A METTL3–METTL14 complex mediates mammalian nuclear RNA N^6-adenosine methylation. *Chem. Biol.* **10**, 93-95 (2014).
49. Abraham, R. T. Cell cycle checkpoint signaling through the ATM and ATR kinases. *Genes Dev.* **15**, 2177-2196 (2001).
50. Deng, C. X. BRCA1: cell cycle checkpoint, genetic instability, DNA damage response and cancer evolution. *Nucleic Acids Res.* **34**, 1416-1426 (2006).
51. Le, D. T. et al. PD-1 blockade in tumors with mismatch-repair deficiency. *Engl. J. Med.* **372**, 2509-2520 (2015).
52. Pardoll, D. M. The blockade of immune checkpoints in cancer immunotherapy. *Rev. Cancer* **12**, 252-264 (2012).
53. Ribas, A. & Wolchok, J. D. Cancer immunotherapy using checkpoint blockade. *Science* **359**, 1350-1355 (2018).

54. Li, Z. et al. N^6-methyladenine in DNA antagonizes SATB1 in early development. *Nature* **583**, 625-630 (2020).
55. Bang, J., Bae, S. H., Park, C. J., Lee, J. H. & Choi, B. S. Structural and dynamics study of DNA dodecamer duplexes that contain un-, hemi-, or fully methylated GATC sites. *Am. Chem. Soc.* **130**, 17688-17696 (2008).
56. Douvlataniotis, K., Bensberg, M., Lentini, A., Gylemo, B. & Nestor, C. E. No evidence for DNA N^6-methyladenine in mammals. *Adv.* **6**, eaay3335 (2020).
57. Jekunen, A. & Vilpo, J. A. 5-Methyl-2'-deoxycytidine. Metabolism and effects on cell lethality studied with human leukemic cells in vitro. *Pharmacol.***25**, 431-435 (1984).
58. Jekunen, A., Puukka, M., & Vilpo, J. Exclusion of exogenous 5-methyl-2'-deoxycytidine from DNA in human leukemic cells: A study with [2-14C]-and [methyl-14C] 5-methyl-2'-deoxycytidine. *Pharmacol.* **32**, 1165-1168 (1983).
59. Vilpo, J. A. & Vilpo, L. M. Nucleoside monophosphate kinase may be the key enzyme preventing salvage of DNA 5-methylcytosine. *Res.* **286**, 217-220 (1993).
60. Zauri, M. et al. CDA directs metabolism of epigenetic nucleosides revealing a therapeutic window in cancer. *Nature* **524**, 114-118 (2015).

Figures

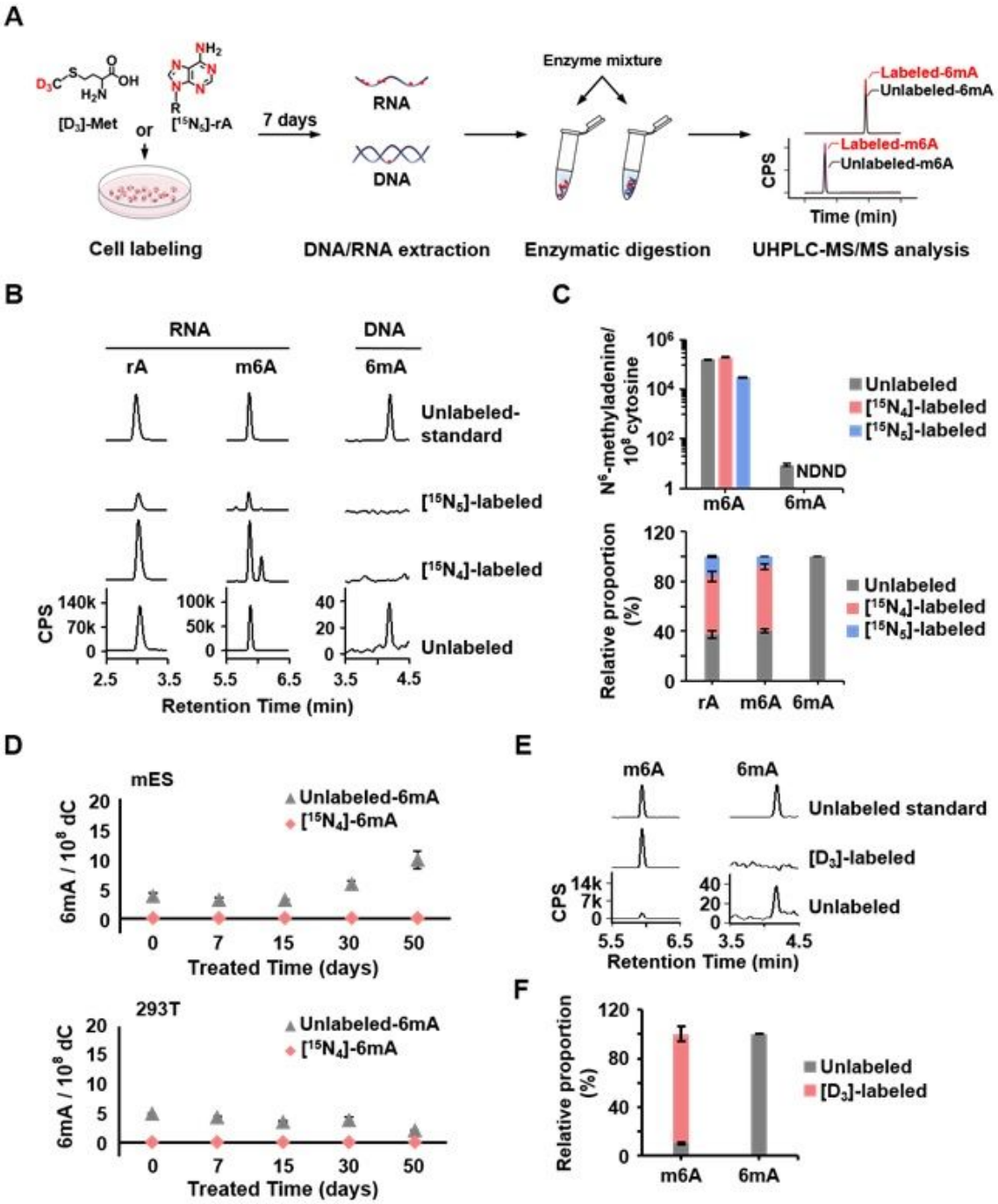

Figure 1

Intracellular degraded RNA m6A cannot be reformulated to generate misincorporated 6mA in genomic DNA. (A) Schematic diagram of heavy stable isotope labeling of RNA m6A and followed UHPLC-MS/MS analysis. (B) UHPLC-MS/MS chromatograms for detection of the labeled rA and m6A in mRNA and the labeled 6mA in genomic DNA of mES cells. mES cells were treated with [15N5]-rA for 7 days. (C) The quantification of m6A in mRNA and 6mA in genomic DNA (the upper) and the labeling percentages of rA, m6A, and 6mA (the lower). (D) The levels of unlabeled-6mA and [15N4]-6mA in genomic DNA of mES cells (the upper) and 293T cells (the lower). The cells were treated with [15N5]-rA for 0, 7, 15, 30, or 50 days. (E, F) UHPLC-MS/MS chromatograms (E) and the labeling percentages (F) of mRNA m6A and genomic 6mA. mES cells were treated with [D3]-L-methionine for 7 days. CPS: counts per second.

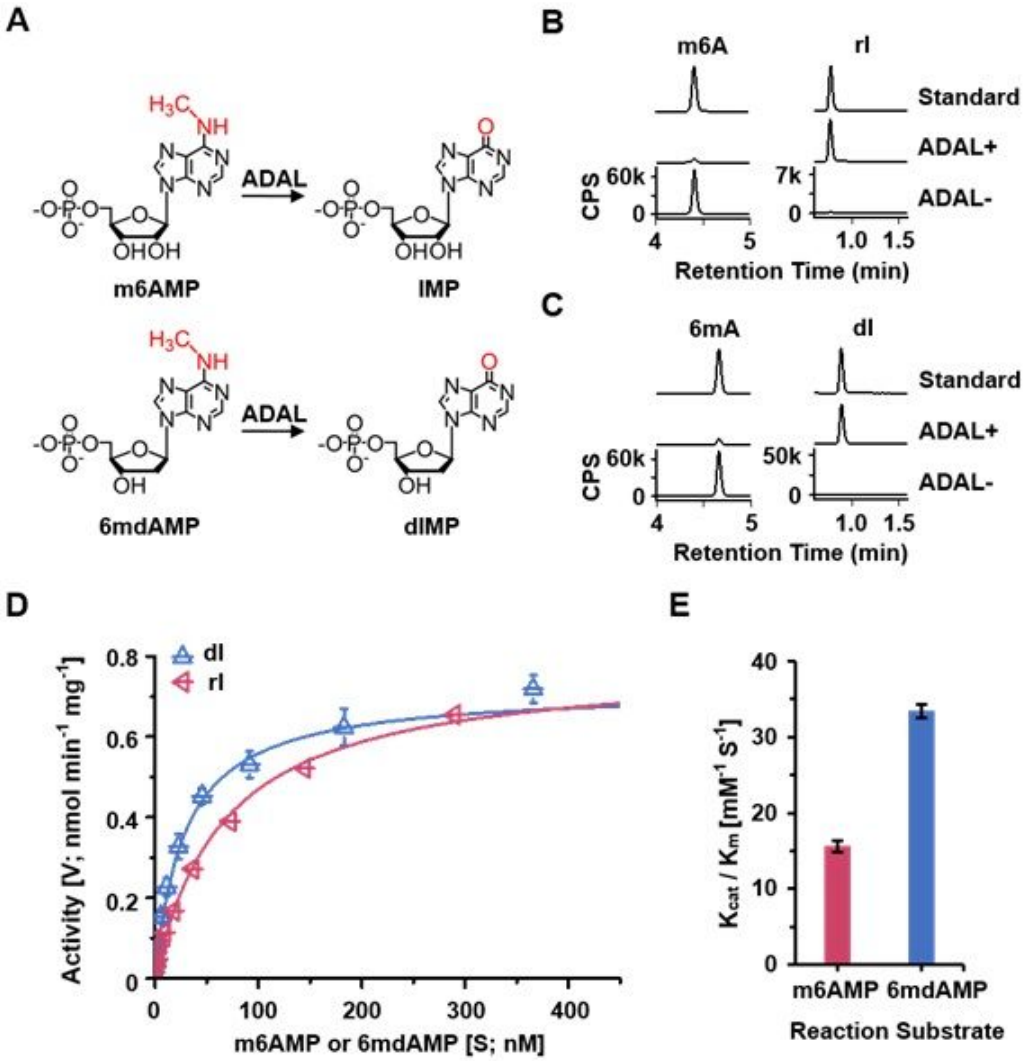

Figure 2

Preferential hydrolysis of 6mdAMP by recombinant ADAL protein in vitro. (A) Diagram of the conversion of N6-methyl-adenosine monophosphate (m6AMP) and N6-methyl-deoxyadenosine monophosphate (6mAMP) into inosine monophosphate (rIMP) and deoxyinosine monophosphate (dIMP) by ADAL, respectively. (B, C) UHPLC-MS/MS chromatograms of m6A and rI from ADAL catalyzing m6AMP (B), and 6mA and dI from ADAL catalyzing 6mAMP (C) in vitro. (D) The determination of kinetic constants for recombinant ADAL catabolizing m6AMP (red) and 6mAMP (blue). The kinetic data were fitted with the Michaelis-Menten equation. Error bars are sd (n = 3 independent analysis). (E) The catalytic efficiency (Kcat/ Km) of ADAL to 6mAMP and m6AMP.

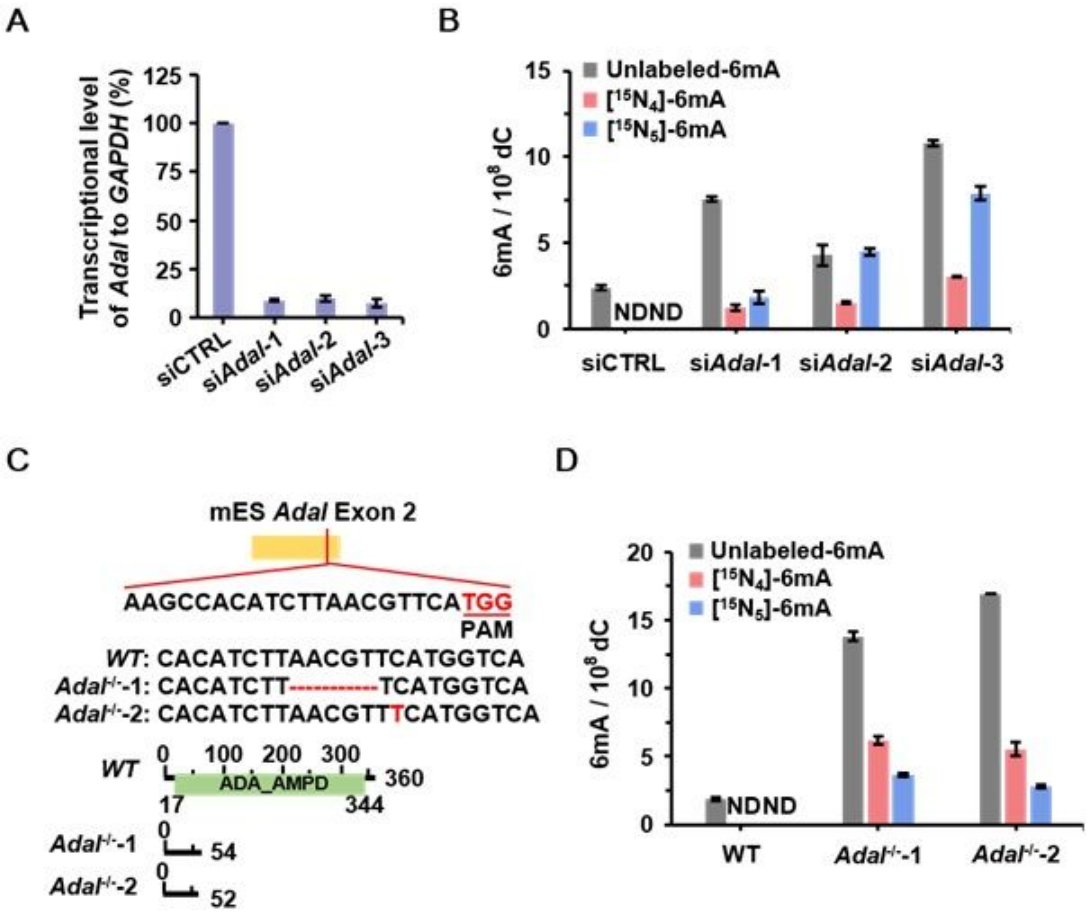

Figure 3

The depletion of ADAL induces misincorporated DNA 6mA in vivo. (A) qPCR confirms the knockdown of Adal mRNA in mES cells. (B) The level of DNA 6mA in [15N5]-rA-treated mES cells after Adal knockdown for 7 days. (C) The sgRNA sequence, knockout sites and representative mutant protein sequences of Adal gene in adal-/- cells. (D) Quantification of genomic 6mA in Adal-/- cells treated with [15N5]-rA for 7 days.

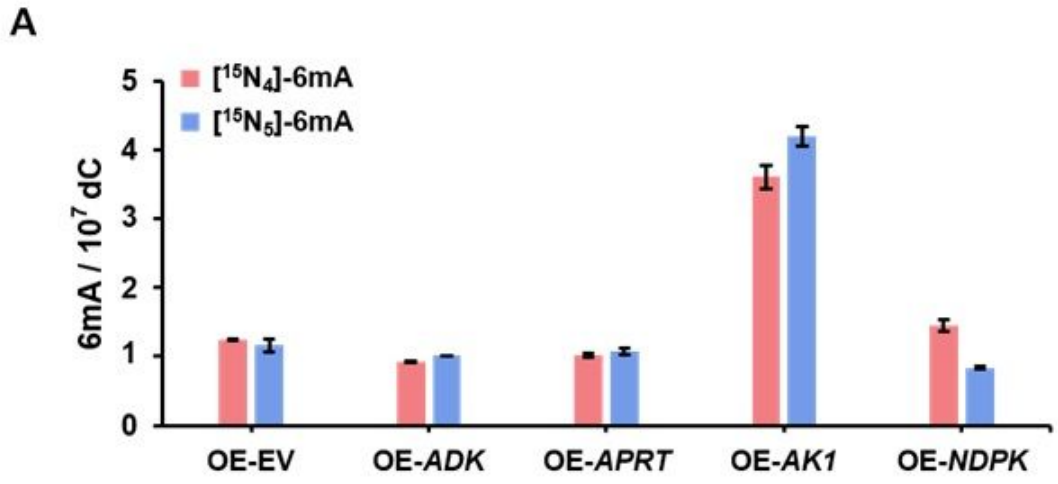

Figure 4

Overexpression of adenylate kinase 1 (AK1) elevates DNA 6mA misincorporation as ADAL is depleted. Quantification of genomic 6mA in [15N5]-rA-treated Adal-/- cells overexpressing ADK, APRT, AK1 or NDPK gene for 7 days.

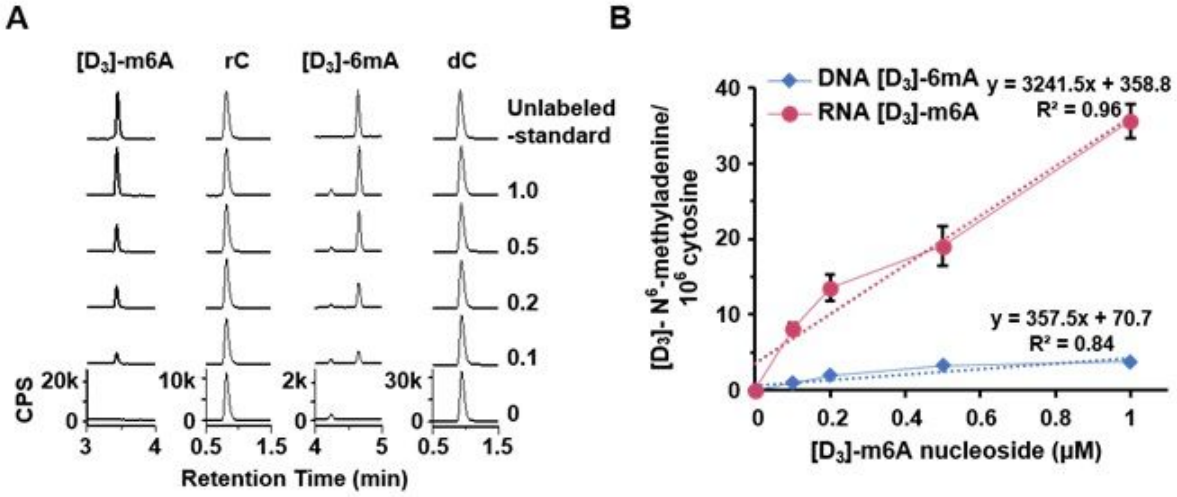

Figure 5

Extracellular m6A nucleoside prefers to being misincorporated into RNA. (A) UHPLC-MS/MS chromatograms of [D3]-m6A in total RNA and [D3]-6mA in genomic DNA of Adal-/- mES cells. (B) The relative misincorporation rate of [D3]-N6-methyladenine in total RNA and genomic DNA of Adal-/- mES cells. Adal-/- mES cells were treated with [D3]-m6A nucleosides at an indicated concentration for 2 days.

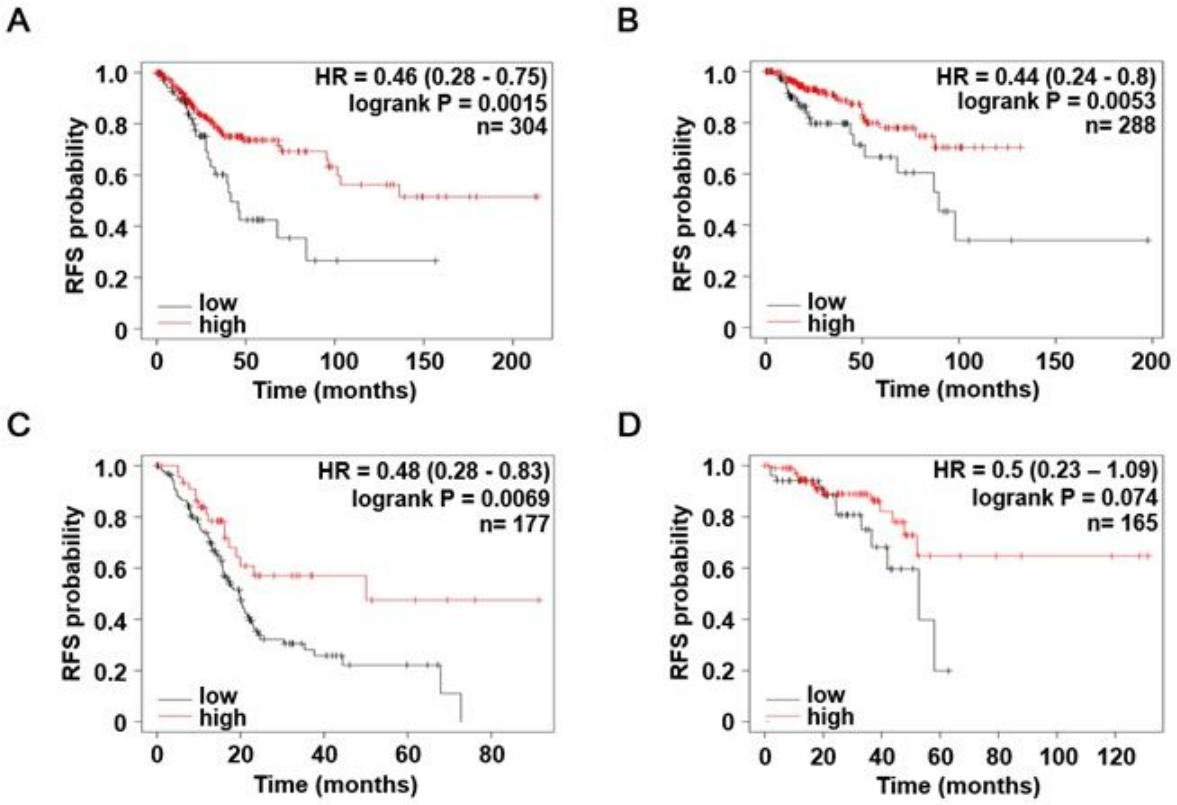

Figure 6

Survival analysis of patients in four cancers according to mRNA expression of Adal. (A) Cervical squamous cell carcinoma; (B) Kidney renal papillary cell carcinoma; (C) Pancreatic ductal adenocarcinoma; (D) Rectum

adenocarcinoma. The Kaplan-Meier survival plots were obtained from http://kmplot.com/analysis/index.php?p=service based on data of the TCGA (The Cancer Genome Atlas) dataset. RFS: relapse free survival; HR: hazardratio; logrank P: log-rank test p-value; n: number of patients with available clinical data;

Supplementary Files

This is a list of supplementary files associated with this preprint. Click to download.

- SIThedeaminaseADALpivotedcatabolismcheckpointsuppressesaberrantDNAN6methyladenineincorporation.docx